ELSEVIER

Nuclear Instruments and Methods in Physics Research A 449 (2000) 446–460

NUCLEAR INSTRUMENTS & METHODS IN PHYSICS RESEARCH Section A

www.elsevier.nl/locate/nima

Straw tube drift-time properties and electronics parameters for the ATLAS TRT detector

T. Akesson[a], A. Antonov[b], V. Bondarenko[b], V. Bytchkov[c], H. Carling[a], F. Dittus[d], B. Dolgoshein[b], N. Dressnandt[e], W.L. Ebenstein[f], U. Egede[a], P. Farthouat[d], D. Froidevaux[d], I. Gavrilenko[g], Y. Grichkevitch[h], Z. Hajduk[k], G. Hanson[i], V.G. Ivochkin[j], S. Jagielski[k], P.T. Keener[e], S. Konovalov[g], V.A. Kramarenko[h], A. Laritchev[h], P. Lichard[d], B. Lundberg[a], F. Luehring[i], S. Muraviev[g], A. Nadtochy[j], P. Nevski[1b], F.M. Newcomer[e], H. Ogren[i], S.H. Oh[f], V. Peshekhonov[c], A. Romaniouk[b,*], D. Rousseau[d], D.R. Rust[i], V. Schegelsky[j], S. Semenov[b], A. Shmeleva[g], S. Smirnov[b], L.N. Smirnova[h], M. Soderberg[a], V. Sosnovtsev[b], E. Spiridenkov[j], M. Stavrianakou[d], F. Tartarelli[d], V. Tikhomirov[g], R. Van Berg[e], C. Wang[f], H.H. Williams[e]

The ATLAS TRT Collaboration

[a]*Fysiska Institutionen, Lunds Universitet, Lund, Sweden*
[b]*Moscow Engineering and Physics Institute, Moscow, Russia*
[c]*Joint Institute of Nuclear Research, Dubna, Russia*
[d]*European Laboratory for Particle Physics (CERN), Geneva, Switzerland*
[e]*Department of Physics and Astronomy, University of Pennsylvania, Philadelphia, Pennsylvania, USA*
[f]*Physics Department, Duke University, Durham, North Carolina, USA*
[g]*P.N. Lebedev Institute of Physics, Moscow, Russia*
[h]*Moscow State University, Institute of Nuclear Physics, Moscow, Russia*
[i]*Indiana University, Bloomington, Indiana, USA*
[j]*Petersburg Nuclear Physics Institute, Gatchina, St. Petersburg, Russia*
[k]*Faculty of Physics and Nuclear Techniques of the Academy of Mining and Metallurgy, Cracow, Poland*

Received 23 November 1999; accepted 14 December 1999

Abstract

The basic drift-time measurement properties of the proportional tubes (straws) of the ATLAS TRT detector and the impact of the parameters of the front-end electronics on performance are discussed. The performance of two different front-end electronics prototypes has been studied in detail at very high counting rate and is reported here.

Keywords: Drift-time accuracy; Straw; Front-end electronics; High counting rate

* Correspondence address: CERN, EP Division, CH-1211 Geneve 23, Switzerland. Tel.: + 41-22-767-1176; fax: + 41-22-767-8350.
E-mail address: anatoli.romaniouk@cern.ch (A. Romaniouk)

[1] Now at Brookhaven National Laboratory, New York, USA.

0168-9002/00/$ - see front matter
PII: S0168-9002(99)01470-9

1. Introduction

The Straw-tube Transition Radiation Detector/Tracker (TRT) in the ATLAS experiment [1] at LHC designed to operate under extremely high-radiation levels. Some of the 425,000 straw proportional tubes of the TRT detector are expected to operate at rates approaching 20 MHz and should nevertheless provide reliable tracking and particle identification information, albeit with reduced efficiency.

The performance of the detector in terms of Transition Radiation (TR) and of its tracking properties, based on drift-time measurements, is defined by many parameters: the TR radiator properties, the detector and straw geometry, the exact gas composition (in particular the xenon gas concentration, the straw operating voltage, the straw gas gain, and the parameters of the signal-processing electronics play an important role in defining this detector performance. In the TRT, gas mixture xenon gas is used to absorb transition radiation photons and has an important impact on the straw response. Once the other parameters are more or less determined, the signal-processing electronics must be optimised to maximise the physics potential of the detector.

Issues concerning the straw detector geometry, the gas mixture and the gas gain to be used for the TRT are discussed in Refs. [2–5], and have led to the specification of the main parameters of the straw detector, which were chosen as a reasonable compromise between many mutually exclusive requirements: cathode diameter of 4 mm, anode wire diameter of 30 μm and gas mixture of $70\%Xe + 20\%CF_4 + 10\%CO_2$.

The dependence of the basic drift-time measurement properties on the electronics parameters had not been reported previously. The primary objectives of the signal-processing electronics may be specified using the following terms that describe the output signal: peaking time, full-width at the base, overshoot area, baseline stability at high counting rate and required minimum operational discriminator threshold. These parameters, that describe the response of the electronics at the channel level, affect the ultimate operational performance of the overall TRT detector, so it is critical that they have a target specification to finalise the design of the front-end electronics.

One peculiarity related to xenon-based gas mixtures should be pointed out. In a high-rate environment, one of the most significant objectives of the front-end electronics is to reliably eliminate the long ion tail from the straw response. The available signal, after this is implemented for the TRT xenon-based gas mixture, is smaller by a factor of 3–5 than for standard Argon-based mixtures (see Section 3). To maintain high-drift-time efficiency at the nominal gas gain ($2.5–4 \times 10^4$ for the TRT), the signal-processing electronics must also be optimised for the lowest possible noise performance. For the same reason, the discriminator threshold used for drift-time measurements will have to be obviously set near the intrinsic noise limit. High-rate operation at very low threshold obviously further strengthens the requirements on the accuracy of the ion-tail cancellation.

The above issues have been studied in detail and the results are presented in Section 3. A baseline approach for the TRT front-end electronics has been implemented in an eight-channel integrated circuit, called the ASDBLR and the results of the measurements are presented in Section 4.

2. Drift-time measurements

The most important tracking characteristics of the straw are its drift-time measurement accuracy and drift-time measurement efficiency. These parameters were measured on a prototype straw tube, exposed to a beam of high-energy pions at the CERN SPS. The set-up included a precise Si-telescope for accurate track position measurement. For high-rate studies, the TRT straw was exposed to a uniform and rate-adjustable ^{55}Fe source, providing reliable data to evaluate the evolution of the performance as a function of the straw counting rate. A detailed description of the experimental set-up can be found in Ref. [6].

The drift-time measurement accuracy and efficiency were obtained by comparing the straw measurement to the extrapolated position of the beam track, determined with an accuracy of 5 μm using the Si-microstrip telescope. Fig. 1 shows the

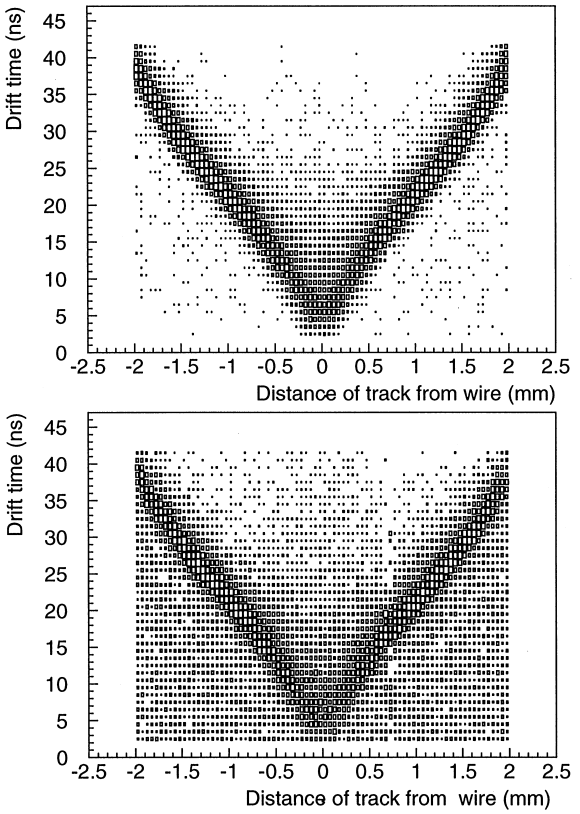

Fig. 1. Measured relationship between drift time (vertical axis) and distance to wire obtained from extrapolation of beam track reconstructed in a Si-microstrip telescope (horizontal axis), for a non-irradiated straw (top) and a at a counting rate of 18 MHz (bottom).

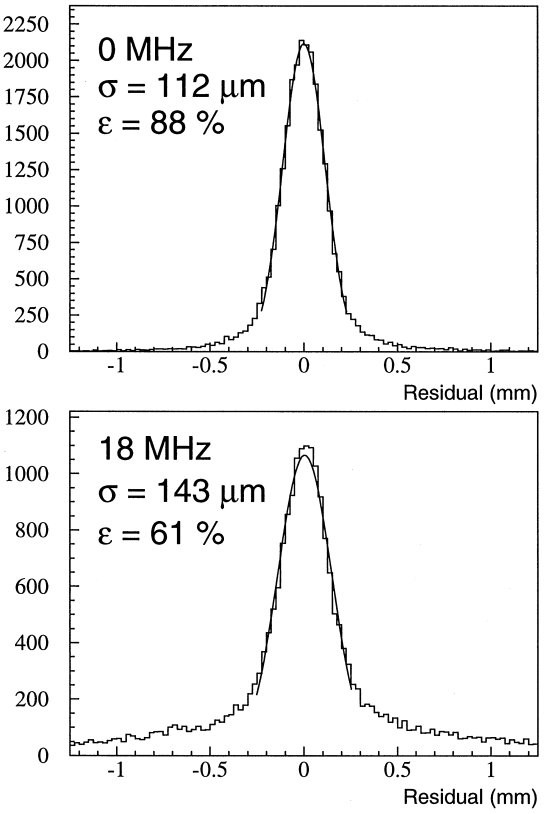

Fig. 2. Distribution of the resulting residual with respect to the beam track, for a non-irradiated straw (top) and at a counting rate of 18 MHz (bottom).

measured drift-time (vertical axis) versus the distance of this extrapolated position of the beam track to the wire (horizontal axis), for straw counting rates of 0 MHz (top) and 18 MHz (bottom). These measurements were performed with a 7.5 ns peaking-time electronics (see Section 3.1.1).

The radius to time (or r–t) relationship in the straw is then obtained by fitting each half of this two-dimensional plot to a third-degree polynomial of the form:

$$r = a + bt + ct^2 + \mathrm{d}t^3.$$

The parameters obtained from the fit are universal and stable for a given gas gain, electronics signal shape and averaged energy deposited in the straw. Once this formula is known, the drift-time measurement can be converted into a distance from the straw wire, and residuals with respect to the position of the extrapolated beam track can be extracted. An example is shown in Fig. 2 for a non-irradiated straws and for straws irradiated at a counting rate of 18 MHz. The drift-time measurement accuracy, σ, and efficiency, ε, are defined from the distributions shown in this figure, respectively, as the rms of a Gaussian fit to the peak and the fraction of selected measurements lying within a range of $\pm 2.5\sigma$ around the peak position. This interval of $\pm 2.5\sigma$ around expected beam track has been chosen as the optimal road width for an accurate track reconstruction in the high-occupancy environment of the TRT. Hits found in the non-Gaussian tail outside this road would not improve the track reconstruction accuracy significantly; in

addition, an increase of the road width would degrade the quality of the track reconstruction at high occupancy. The method described here is used throughout the following sections to evaluate the drift-time measurement accuracy and efficiency as a function of the analogue signal output parameters and of the straw counting rate. It is important to note that the straw hit efficiency is at least 97% for the straw tubes foreseen for the TRT and that it is essentially the $\pm 2.5\sigma$ requirement on the residual which restricts the drift-time efficiencies reported here to the values shown.

3. Straw drift-time properties and front-end electronics parameters

3.1. Straw signal characteristics and requirements on front-end electronics

A nearly exact replication of the straw output signal due to a point-like ionisation deposited in the chosen Xe-based gas mixture is shown in Fig. 3. An accurate parameterisation of this signal can be found in Refs. [4,6]. The time development of the signal observed on the anode wire is characterised by an initial burst of current (electron component), that comprises 3–5% of the total charge integrated over the full positive ion drift time of 60 μs, and a remaining, signal (ion tail) largely controlled by the motion of the much heavier ions as they move towards the cathode. For argon-based gas mixtures this signal is well predicted by an equation that includes the effects of the electric field, chamber geometry, and ion mobility [7]. Unfortunately, the time development of the signal, when the TRT xenon-based gas mixture is employed, cannot be accurately described in this fashion, which indicates the presence of additional processes such as the creation of semi-stable negative ions in the avalanche. As can be seen from Fig. 3, appreciable current continues to flow several hundred nanoseconds after the initial pulse of current. At the design luminosity of the LHC, the front-end electronics will have to efficiently process several such signals, broadened by the extended arrival time of drift electrons from tracks and different in magnitude by as much as a factor of 10, over the 200 ns

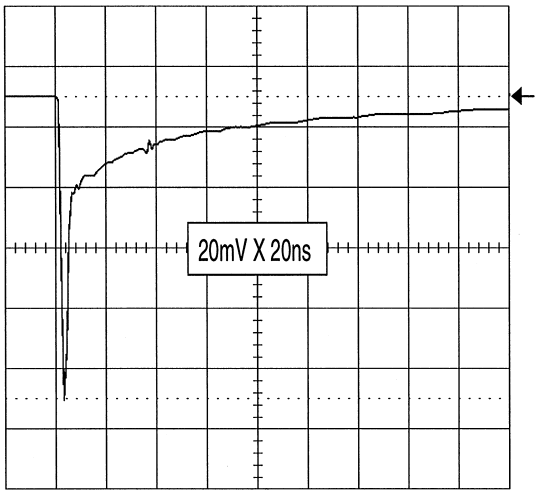

Fig. 3. Straw output signal typical of a point-like ionisation measured at the wire anode for the 70%Xe + 20%CF_4 + 10%CO_2 gas mixture chosen for the ATLAS TRT tracker.

time window shown in the plot. For this reason, a precise elimination of the ion tail is one of the most crucial goals of the front-end electronics design.

To achieve an accurate ion-tail cancellation, the electronics takes advantage of the rapid onset of the avalanche signal, by employing a passive network that sharply differentiates the chamber signal. The overshoot from the differentiation network is designed to mirror the current from the decaying ion tail so that the sum of the suppressed ion tail and overshoot current is zero. This results in an early return to baseline of the output signal. In the xenon-based gas mixture, the electron component of the chamber signal described above provides the primary current for this differentiation process. Since the electron signal comprises such a small part of the total ionisation charge, it is far more difficult to provide accurate cancellation than for the more typical argon-based mixtures, for which as much as 15% of the total charge may be used to help cancel the long ion tail.

It is also important to note that the maximum gas gain allowing stable operation in a Xe-based gas mixture is limited by the onset of streamer-mode avalanche events, which increase rapidly in

rate with the gas gain, space-charge effects in the avalanche, and possibly ageing effects (see for example, Refs. [3,4]). These considerations limit the maximum gas gain to about 4×10^4 for a 30 μm anode wire. In order to guarantee stable operation system wide over many years, the nominal gas gain has been chosen to be 2.5×10^4. This operational limit on the gas gain, coupled with the need to trigger on the avalanche signal from the first few drift electrons, argues strongly for careful consideration of both extrinsic and intrinsic noise in the choice of technology and design of the front-end electronics.

3.2. Parameterisation of the signal shape

The straw drift-time measurement accuracy is very sensitive to the shape of the output signal presented to the discriminator. The most important parameters defining the signal shape are peaking time, base-to-base width and overshoot area, as illustrated in Fig. 4.

3.2.1. Peaking time

The peaking time is defined as the time it takes the processed straw signal from a point-like energy deposition to rise from 1% to 100% of its maximum amplitude. Statistical variations in the number of primary electron–ion pairs created by charged particles result in a peaking-time-dependent trigger slewing, which may degrade the drift-time measurement accuracy.

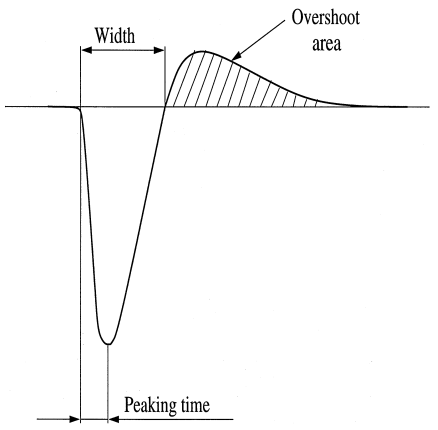

Fig. 4. Parameters of *the processed* straw signal at the input to the discriminator.

Detailed studies of the straw drift-time measurement properties have been performed in a test beam using discrete analogue electronics with a variable peaking time. The main results of these studies are shown in Figs. 5 and 6, where the drift-time measurement accuracy and efficiency, are shown as

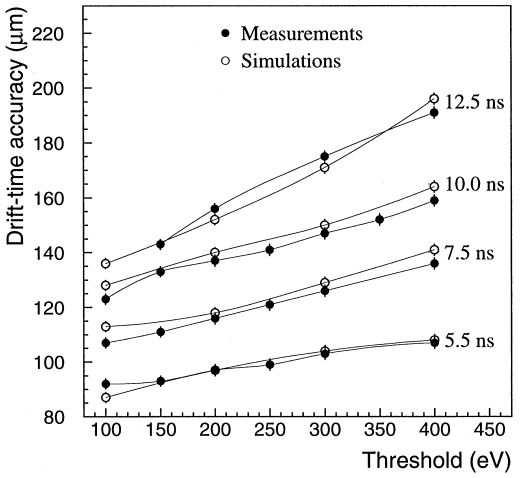

Fig. 5. Drift-time measurement accuracy as a function of the electronic threshold for different signal peaking times. The test-beam measurements are compared to simulations of the straw response.

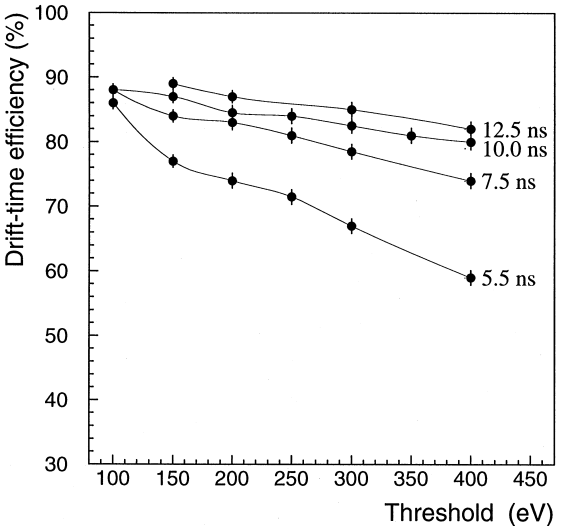

Fig. 6. Drift-time measurement efficiency, as defined in the text, as a function of the electronic threshold for different signal peaking times.

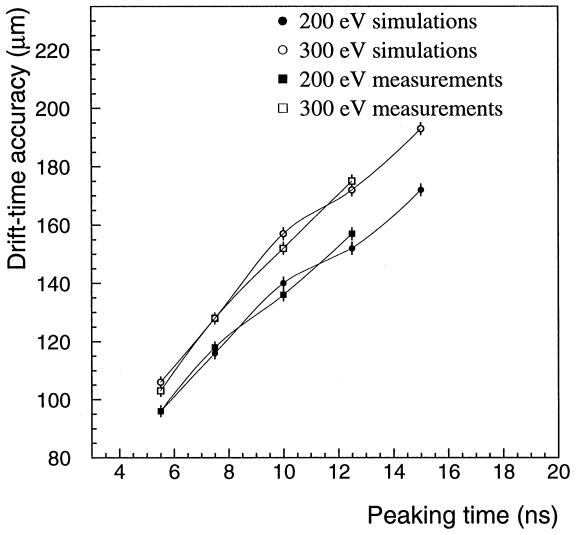

Fig. 7. Drift-time measurement accuracy as a function of peaking time for different electronic thresholds. The test-beam measurements are compared to simulations of the straw response.

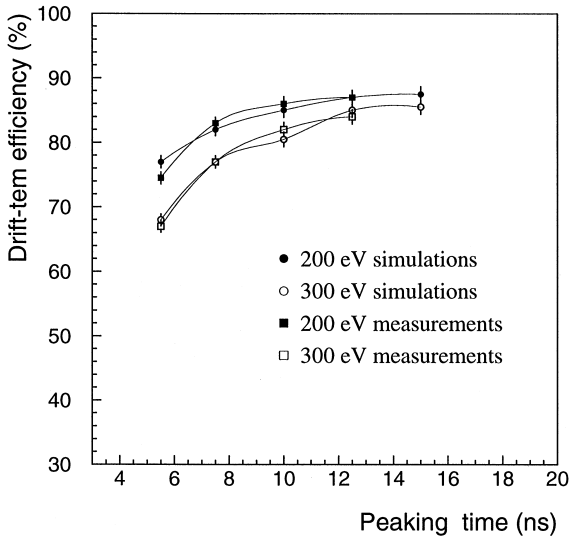

Fig. 8. Drift-time measurement efficiency, as defined in the text, as a function of peaking time for different electronic thresholds. The test-beam measurements are compared to simulations of the straw response.

a function of the electronic threshold, given in absolute scale (eV) for different peaking times. Other representations of these data are shown in Figs. 7 and 8.

These figures also show that detailed Monte-Carlo simulations of the experimental measurements [4] describe the test-beam data quite accurately over a wide range of values for the peaking time and the electronics threshold.

The results for different peaking times shown in Fig. 5, indicate that a drift-time measurement accuracy of better than 100 μm can be obtained for a peaking time of 5 ns and for an electronic threshold below 300 eV. However, as shown in Figs. 6 and 8, the drift-time measurement efficiency as defined in Section 2, decreases rapidly for peaking times below 7.5 ns, mainly because of non-Gaussian tails similar to those shown in the distributions of Fig. 2.

Due to properties of the circuit devices, of the interconnect and of the straw tube, the intrinsic noise of the preamplifier and shaping circuit is dominated by *series* noise for peaking times below 10 ns, and increases at a rate approximately proportional to the inverse of the square root of the peaking time. The increase in intrinsic noise for very fast peaking times is compounded by stability issues that accompany very high bandwidth systems. The studies shown above demonstrate that the optimal peaking time is close to 8 ns, corresponding to a drift-time measurement accuracy of 120 μm for a threshold of 200 eV and a gas gain of 2.5×10^4. This threshold corresponds to an equivalent input charge of about 15 000 electrons (in the first 8 ns) and to a threshold-to-noise ratio of at least 5.5 : 1. Operation at lower thresholds is, in principle, possible for an individual straw and electronics channel but appears to be unrealistic for a large system such as the TRT.

In conclusion, the front-end electronics specifications have been set to 8 ns for the peaking time and 200 eV for the corresponding operational threshold, applied to the discriminator.

3.2.2. Signal width

The second parameter defining the analogue output signal in Fig. 4 is its width. It is defined as the full-width of the signal at its base, i.e. at 1% of its amplitude. In principle, this width should be as short as possible to minimise the overlapping of signals from adjacent LHC bunches, which are 25 ns apart. Since the peaking time is already

specified to be about 8 ns, the minimisation of the pulse width is a matter of making the pulse at the output of the shaper as symmetric as possible. The multi-pole equivalent shaping implemented in the ASDBLR has demonstrated that a pulse width of as small as 20 ns is achievable, for straw signals from a point-like ionisation source similar to that shown in Fig. 3.

Another constraint on the output signal width arises from the required amplitude uniformity for energy depositions along the length of the straw. This determines to some extent the electron identification performance. The unterminated TRT straw signal has both direct and reflected components. In the most difficult case, namely for depositions near the amplifier in the 75 cm long barrel TRT straws, these components may be separated by as much as 6–7 ns. A position-dependent amplitude variation of as much as a factor of two has been measured for a signal width of 10 ns. The test-beam data have shown that the electron identification performance of the straws is not significantly affected if the overall position dependence of the output signal amplitude below $\pm 20\%$. In order to keep the contribution from the amplitude variations along the straw below $\pm 10\%$, the output signal width of the front-end electronics has to be above 18 ns.

The maximum length of the straw response corresponds to a charge particle crossing the straw near the wire, thus generating primary electrons which may drift to the wire over maximum drift time of 42 ns (in a magnetic field of 2 T), to which should be added the 6–7 ns quoted above and needed to collect the direct and reflected components of the signal. The straw response to the arrival of the secondary electron clusters at the wire is a series of superimposed avalanche ionisations, each with the shape shown in Fig. 3. While the maximum spread of arrival of ionisation pulses at the amplifier is about 48 ns, the extended ionisation signal from a charged particle track is typically much shorter. The test-beam measurements show that the average signal width due to ionising tracks is only 5 ns wider at the base than that due to point-like ionisations for an output signal width of 20 ns. A further decrease of the signal output width would not reduce significantly the average signal width due to ionising tracks and therefore would not improve essentially the straw occupancy from neighbouring bunches at high luminosity.

3.2.3. Overshoot

For the shaping chosen for the TRT electronics, the fast component of the output signal is normally followed by a slower component of opposite polarity or overshoot, as shown in Fig. 4. To provide a stable trailing edge for the discriminator output, the area of this overshoot should be at least 5% of the fast component of the signal. On the other hand, too large overshoot area would result in a degradation of the straw drift-time accuracy and efficiency at high counting rate, since signals arriving while there is a significant residual overshoot from a previous pulse will require increased amplitude to exceed threshold. The magnitude of this degradation depends on the area and width of the overshoot and has been studied in detail with simulations.

These simulation studies were performed to specify quantitatively the acceptable area and width of the overshoot. As an example, results from simulations of the drift-time accuracy as a function of the straw counting rate for front-end electronics with a 12.5 ns peaking time are presented in Fig. 9. These simulations have shown that the most important parameter characterising the overshoots is its relative area, with respect to the fast signal component. On the contrary, the exact duration of the overshoot signal does not have a significant impact on the measured drift-time accuracy. As demonstrated in Fig. 9, the drift-time accuracy can be maintained below 200 μm at a counting rate of 14 MHz, typical of operation at high luminosity, only if the relative area of the overshoot is less than 20%. The disciminator triggering efficiency was not found to depend crucially on this overshoot area if it is below 20%. As a result, the front-end electronic specification for the output signal overshoot is that its relative area must be between 5% and 20% of the fast signal component for the average signals expected from minimum-ionising charged particles.

3.2.4. Very large signals

A final important consideration for the front-end signal shaping is the recovery time needed for very

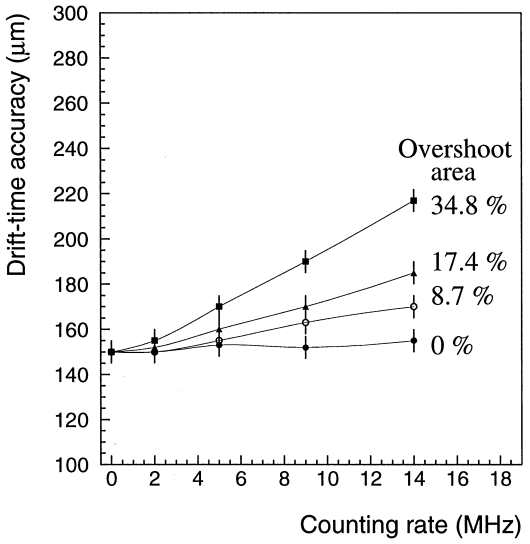

Fig. 9. Drift-time measurement accuracy as a function of the straw counting rate for different overshoot areas of the analogue output signal as obtained from simulations front-end electronics with a 12.5 ns peaking time.

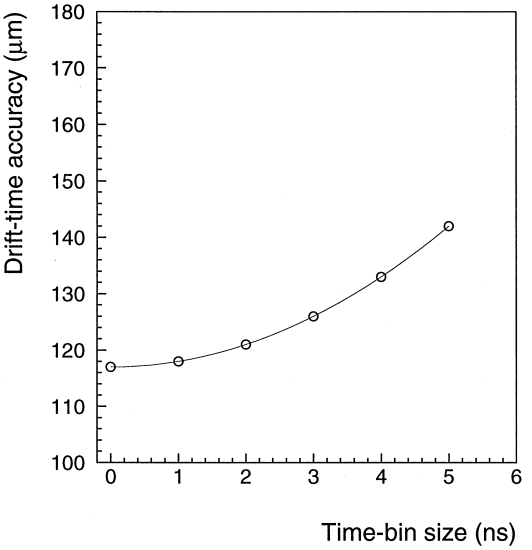

Fig. 10. Drift-time accuracy measured as a function of the time-bin size of the TDC.

large charge depositions induced by streamer mode avalanches or large charge depositions by neutrons or other particles. Although rates for these kinds of depositions are not expected to be large in the ATLAS TRT, normally ≈ 10 kHz per straw [1]), the long ion tail that accompanies these events can potentially disable the shaping circuit for periods up to several microseconds, once the tail cancellation networks are saturated. An optimal circuit should minimise the deadtime, maintaining it below 1 μs for depositions of more than 1000 times the normal threshold of 200 eV.

3.3. Determination of optimal time bin width

The drift-time measurements described above were performed with a TDC with a time-bin size of 0.25 ns. Cost considerations make it highly desirable to limit the bandwidth burden of the front-end electronics on the DAQ system to the minimum compatible with the performance requirements. The time-bin width, which is inversely proportional to the readout bandwidth, has therefore been chosen on the basis of its impact on the drift-time measurement accuracy. The bin size for drift-time measurements was chosen on the basis of its impact on timing accuracy. Fig. 10 shows the measured drift-time accuracy as a function of the time-bin size of the TDC for the analogue front-end electronics parameters specified above.

At the LHC, the time between bunches is 25 ns and the data from the detector are pipelined in 25 ns bins [5], while they await the validation of the level-1 trigger. The TRT readout protocol requires three time slices to be read out for each straw, after the level-1 trigger has been accepted. Within each 25 ns time slice, the drift-time information can be coded into a certain number of bits. Two bits per time slice would result in a 6.25 ns time-bin size, which would lead to an unacceptable degradation of the drift-time accuracy. As shown in Fig. 10, a more precise coding into three bits per time slice, resulting in a 3.13 ns time bin would lead to no more than a 15 μm degradation of the drift-time accuracy. The front-end electronic specification for the time-bin size has therefore been set to 3.13 ns, i.e. $\frac{1}{8}$ of a 25 ns interval.

4. Description of front-end circuits

As mentioned above, the output signal from a straw operating with a Xe-based gas mixture has

a very long ion tail (lasting up to 60 μs). Precise ion-tail cancellation therefore has to be implemented in the analogue front-end electronics for reliable and efficient operation at the very high counting rates expected at the LHC design luminosity. Various compensation techniques have been studied and implemented in discrete electronics and in integrated circuits over the past few years [4,6,8]. The main conclusion from these studies was that a pole/zero cancellation network with realistic parameters cannot provide alone stable operation of the electronics at very high counting rate, and an active baseline restoration is therefore needed. Two approaches with active baseline restoration have been developed and tested extensively: a DC-coupled circuit, based on discrete elements and recently produced as a pilot chip, and an AC-coupled integrated circuit, the ASDBLR, which is the baseline front-end analogue chip for the TRT.

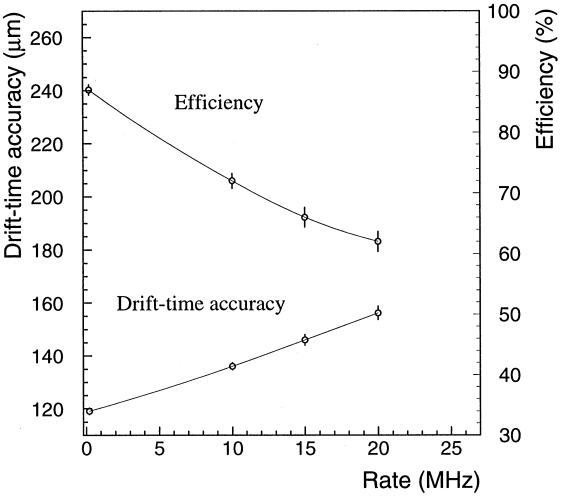

Fig. 11. Drift-time measurement accuracy (left-hand scale) and efficiency (right-hand scale) as a function of the straw counting rate for the DC-coupled analogue circuit with baseline restoration.

4.1. DC-coupled front-end electronics

The design principles of this electronics circuit have been described in Ref. [6]. The most salient feature of this approach is in the baseline restorer, which is functionally the same as the well-known Robinson restorer, where the differentiation with a decoupling capacitor has however been replaced by an integration in the negative feedback chain. This allows the use of more complex differentiation schemes and improves the linearity of the response. Initially, this approach was implemented in a circuit based on discrete elements. The output signal parameters were set according to the specifications defined above: a peaking time of 8 ns, a width at the base of 20 ns and an overshoot area of 13%.

The test-beam measurements with this circuit connected to a single straw are shown in Fig. 11 as a function of the straw counting rate. Even at the highest counting rates of about 20 MHz expected for the TRT straws at the LHC design luminosity, the straw drift-time measurement performance remains quite respectable: the drift-time accuracy is about 155 μm (compared to 120 μm at low counting rate) and the drift-time efficiency is about 60% (compared to 87% at low counting rate). This circuit, based on discrete elements, has been very useful to fine-tune the specifications, and the results shown in Fig. 11 should be treated as a goal to be approached as closely as possible by the final version of the radiation-hard analogue front-end integrated circuit.

4.2. AC-coupled front-end electronics: the ASDBLR chip

4.2.1. Principle

Another approach was used in the design of a full-custom, analogue, bipolar ASIC, the ASDBLR chip, which is the current baseline front-end electronics chip for the ATLAS TRT. It provides eight channels of amplifier, shaper, baseline restorer and discriminator on a 6.17 mm × 4.78 mm silicon substrate and is described in Ref. [8]. The block diagram of the ASDBLR is shown in Fig. 12, and indicates the main architectural features of the circuit. The design of this chip is nearly finalised and therefore warrants a detailed description of its function and performance.

4.2.2. General description

The requirements for the TRT front-end electronics partly discussed above led to the choice of a largely differential circuit which includes ion-tail

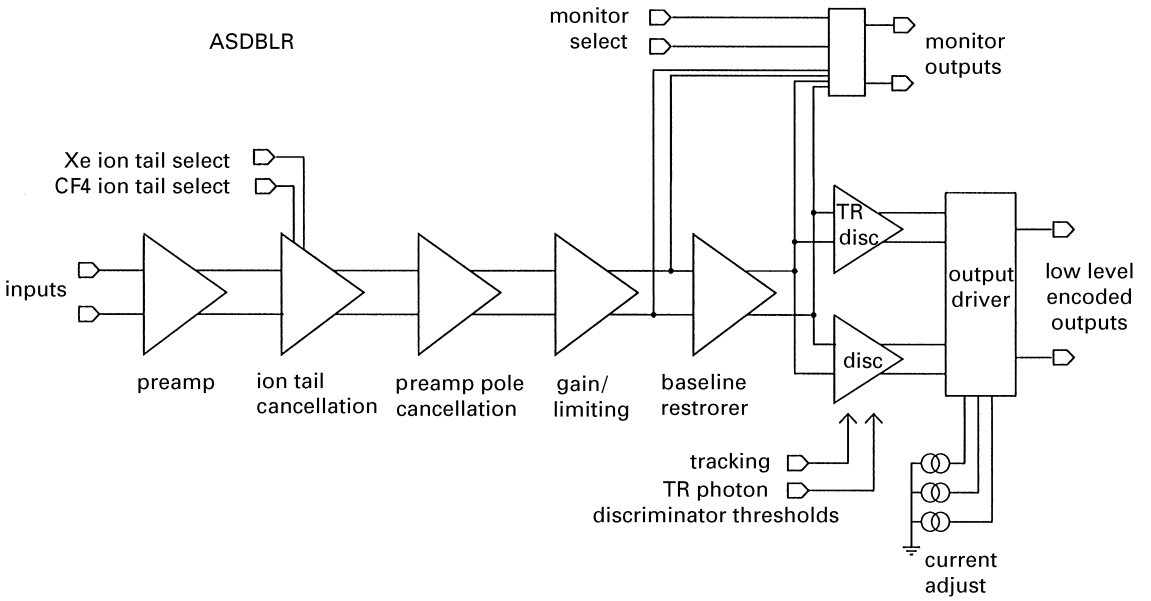

Fig. 12. Block diagram of the ASDBLR chip.

compensation and a capacitively coupled diode-clamped baseline restorer. Separate high (10 fC range) and low (150 fC range) sensitivity discriminators allow both tracking and TR photon detection for each channel. The ion-tail cancellation circuit can be chosen by the user to be compatible with either Ar (or CF_4) or Xe-based gas mixtures.

4.2.3. Preamplifier and shaper

Each channel of the ASDBLR has dual preamplifiers that provide a balanced DC input to the shaper as well as some measure of common-mode rejection. The two active inputs per channel are bonded to the package allowing the common-mode rejection to be extended off the chip.

Since the straws in the TRT are unterminated at the opposite end, the preamplifier must provide a reasonable termination in order to avoid multiple reflections of the signal. The input of the ASDBLR has been designed to provide a good termination and to maximise the usable signal charge by careful consideration of the spectral behaviour of the input impedance. Since most of the useful signal from the straw is collected in the first few ns, the circuit is designed so that the input impedance falls off with frequency. In the fabricated design, the input impedance is relatively uniform at 290 Ω up to 3 MHz and falls to 70% of this value at 14 MHz. The measured impedance versus frequency of the ASDBLR input is shown in Fig. 13. Measurements with a real straw [9] have shown good termination

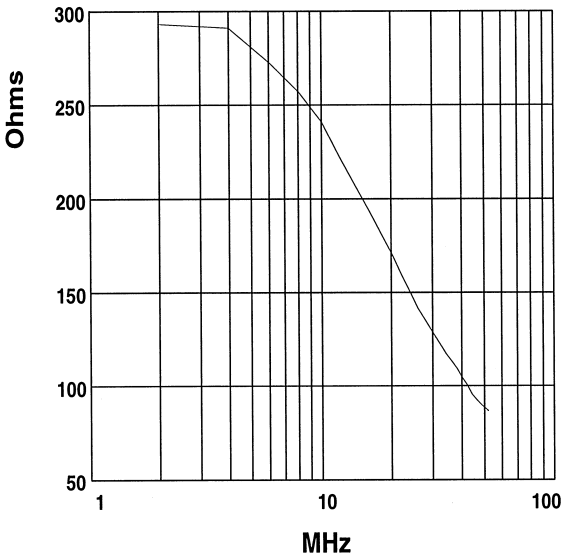

Fig. 13. Measured ASDBLR input impedance versus frequency.

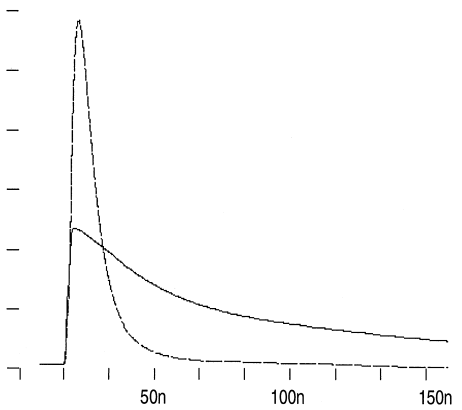

Fig. 14. SPICE simulation of the ASDBLR output of the preamplifier (solid) and shaping circuits (dashed). The horizontal scale is given in ns.

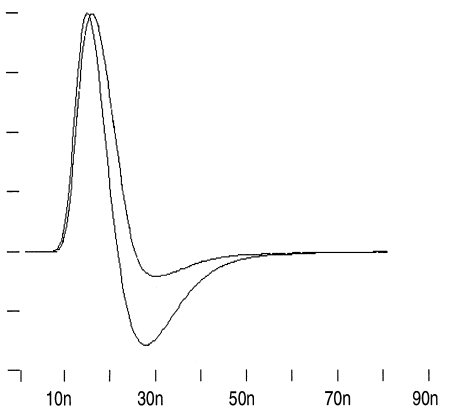

Fig. 15. SPICE simulation of the ASDBLR output after baseline restoration for input charges of 2 fC (with large undershoot) and 25 fC (rescaled). The horizontal scale is given in ns.

properties of the input stage of the preamplifier and no significant reflections have been observed.

The peaking time of the shaper has been set close to 7.5 ns, as required for optimal performance (see Section 3.2.1). Typical process variations are expected to change the peaking time by 1 ns or less. Fig. 14 shows the SPICE-simulated response of the circuit for a point-like ionisation at the output of the preamplifier (solid line) and of the shaper (dashed line). The long ion tail typical for Xe-based gas mixtures is evident in the preamplifier trace. The cancellation network in the shaper eliminates most of this extraneous signal, providing fast recovery for good double pulse resolution and minimal internal pile-up. Differential design techniques within the chip, with pseudo-differential inputs and differential outputs, along with substrate barriers between channels and hierarchical power-bussing result in a high isolation between channels. On-chip cross-talk between channels has been measured to be less than 0.2%.

4.2.4. Baseline restorer (BLR)

As discussed in previous sections, the operation at very high rates of a circuit without active baseline restoration may result in an unstable threshold due to pile-up caused by imperfections in the ion-tail cancellation or by long integration times in other circuit elements. This may lead to several microseconds of uncertain threshold or even persistent triggering due to large energy depositions which saturate the tail cancellation network and leave the slowly decaying ionisation current uncompensated. Active baseline restoration completely eliminates all residual tails and guarantees stable operation at high rate, as illustrated by SPICE simulation in Fig. 15. A capacitively coupled diode shunt restorer with a relatively short recovery time constant has been implemented to limit these effects. The signal from the differential shaper is coupled into the BLR through a series-connected, 8 pF, capacitor pair, as schematically shown in Fig. 16. A diode, connected to virtual

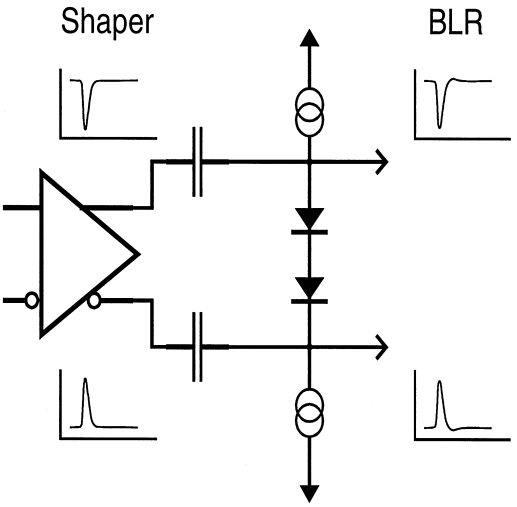

Fig. 16. Illustrative schematic of the baseline restorer (BLR).

ground on the output side of each capacitor, provides a CR differentiation of the signal with a variable time constant. The diode current is set to 40 μA to provide a 5 ns differentiation time constant in quiescent mode. The exponential behaviour of the diode junction is used to moderate the diode impedance as the signal is processed. The time constant is increased as the desired lobe of the signal passes through, and dramatically lowered when the signal returns to baseline to reduce the overshoot required to recharge the capacitors.

Fig. 15 shows the shape of the signal at the BLR output for both a minimal 2 fC signal and an average 25 fC signal rescaled to the 2 fC signal. Since larger signals drive the diode clamp into a high impedance mode, they discharge the capacitance by a proportionally smaller amount and have a smaller fraction of overshoot, as demonstrated in Fig. 15.

4.2.5. Dual discriminator

The BLR output is connected to a fast discriminator with sufficient hysteresis to guarantee a 4–5 ns minimum output width. If one includes the effects of off-chip drivers/receivers, the deadtime is about 5 ns. As mentioned in Section 3.2.2, for the unterminated TRT straws, a relatively fast shaping would degrade the energy measurement critical for detecting transition radiation photons, due to the delay in arrival of the reflected signal. To minimise this effect and improve the TR performance, the peaking time was increased from 7.5 to 12 ns before the high-level discriminator. This extra shaping time allows more efficient integration of the direct and reflected TR photon signals, which reduces the effective threshold spread for depositions along the length of the straw. The output of the two discriminators is encoded into a programmable bi-level output current. Fig. 17 shows

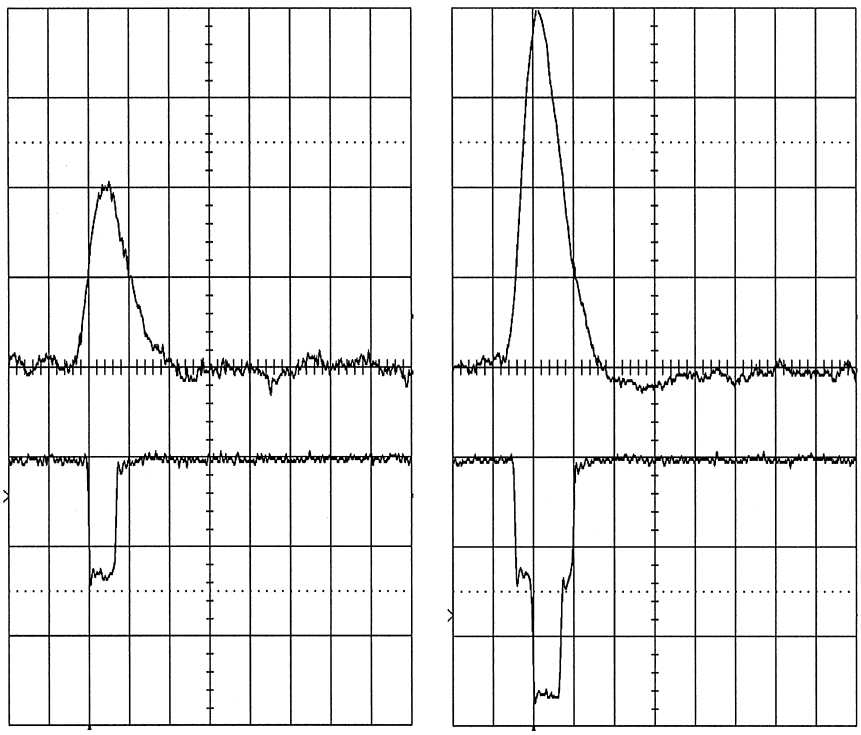

Fig. 17. Output of shaper (top) and discriminator (bottom) of ASDBLR chip connected to a TRT straw. The plot on the left (right) corresponds to a signal below (above) the threshold for the TR discriminator. Each division corresponds to 20 ns for the horizontal scale and 25 mV (discriminator outputs) for the vertical scale. Vertical scale for shaper outputs is arbitrary.

the ^{55}Fe response of the ASDBLR shaper (upper trace) and dual discriminator (lower trace), when connected to a 4 mm diameter straw filled with a xenon-based gas mixture.

The shaper signal on the left-hand plot is below the high-level threshold and produces a single-level discriminator output 15 ns wide. The five times larger signal on the right-hand plot is well above the high-level threshold and produces two levels of discriminator output.

Thresholds can be set from below the noise level to 1 keV for the low-level discriminators and from 1 to 15 keV for the high-level discriminators.

4.3. Measured performance

Several ASDBLR chips have been measured to determine channel-to-channel uniformity. The relation between the input signal amplitude and the discriminator threshold current is plotted in Fig. 18 for 16 different channels. One can see that a 47 μA threshold corresponds to a 250 ± 25 eV energy threshold for all 16 channels. For the high-level threshold, the uniformity is measured to be even better than the $\pm 10\%$ uniformity measured for the low-level threshold, as shown in Fig. 19.

As mentioned above, the ASDBLR design has been optimised to maximise the signal-to-noise ratio. The noise properties of the chip have been measured with one channel connected to a straw through a short cable (5 cm) and a LEMO connector. The noise counting rate for different thresholds has been measured and is shown in Fig. 20. At a nominal threshold of 200 eV, for which the measured straw hit efficiency without the drift-time

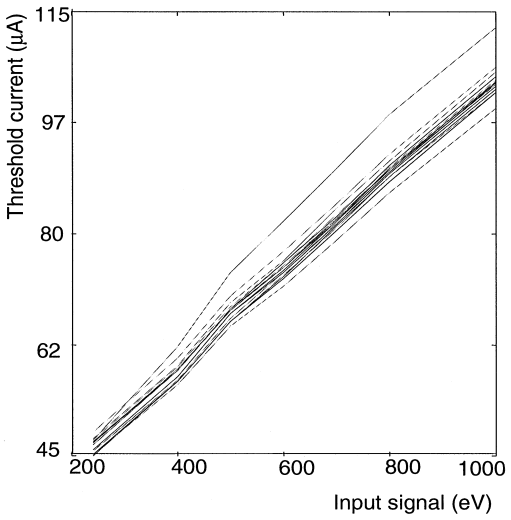

Fig. 18. Low threshold current versus signal amplitude for 16 different channels of two ASDBLR chips.

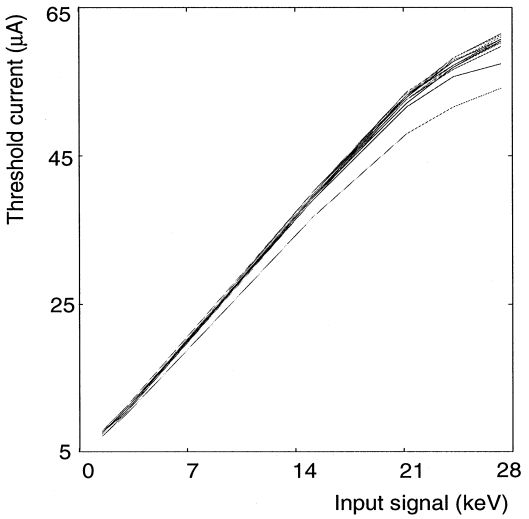

Fig. 19. Same as Fig. 18 for the high-level threshold.

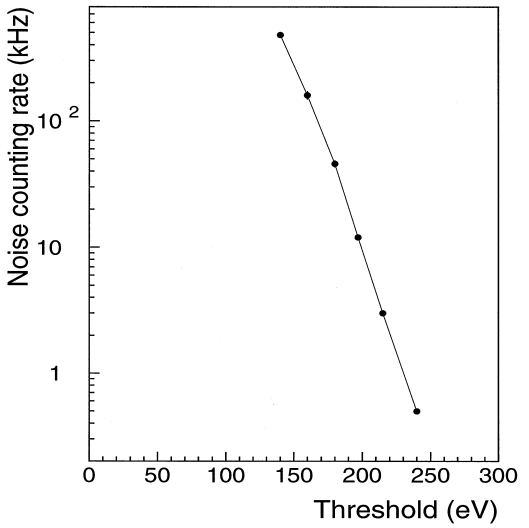

Fig. 20. Noise counting rate as a function of the low-level threshold for one channel of an ASDBLR chip connected to a straw through a 5 cm long cable with LEMO connectors.

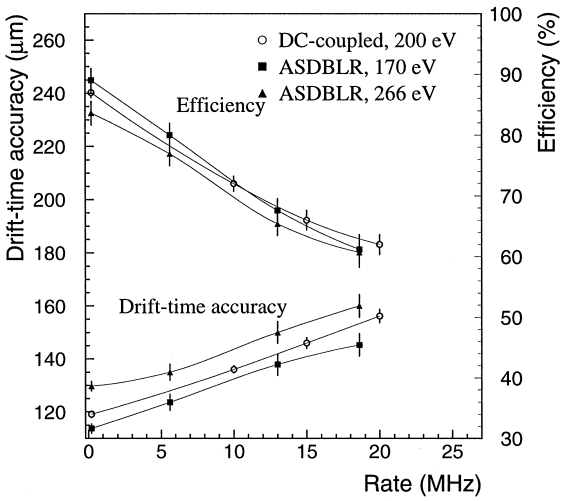

Fig. 21. Drift-time measurement accuracy (bottom) and efficiency (top) as defined in Section 2, as a function of the straw counting rate measured for the DC-coupled electronics at a low-level threshold of 200 eV and for the ASDBLR chip at low-level thresholds of 170 and 266 eV.

measurement requirements is 97%, the noise counting rate is measured to be less than 10 kHz.

The ASDBLR performance has been studied at high counting rates (up to 18.6 MHz) and compared to the discrete component (DC-coupled) reference circuit described in Section 4.1. The results, shown in Fig. 21 as a function of the straw counting rate, indicate that the ASDBLR matches the performance of the hand-tuned reference circuit, except perhaps for the drift-time efficiency at counting rates above 15 MHz which is somewhat lower for the ASDBLR chip.

The overshoot area for the ASDBLR chip depends strongly on the absolute signal amplitude as shown in Fig. 15 and therefore on the gas gain (see also Section 4.2.4). The measured area of the overshoot is about 27% of the area of the 2 keV primary signal. At the nominal gas gain, the overshoot area therefore exceeds the specified maximum value of 20%. This turned out not to be a problem for the high-rate studies presented here, since the gas gain had to be increased by about 50% to eliminate system noise coming from the relatively large straw matrix capacitance in the experimental set-up [6]. The operation at higher gas gain led to a reduction of the overshoot area from 27% to about 18% and, hence, to somewhat better results than would have been obtained at the nominal gas gain. The second generation of the BLR circuit, similar in principle to the first, is expected to significantly reduce the overshoot area for small signals and should therefore allow operation at the nominal gas gain with the same high-rate performance, shown in Fig. 21.

5. Conclusions

The TRT performance in the ATLAS experiment at the LHC will very strongly depend not only on the detector parameters (global detector design, straw chamber design, gas composition, high voltage, etc.), but also on the front-end electronics parameters. Extensive studies of the drift-time measurement properties of the TRT straws equipped with discrete electronics comprising components with variable parameters has resulted in clean specification for the following design parameters of the TRT front-end electronics:

Peaking time:	7.5 ns
Shaper output width:	20 ns
High-rate stability:	AC-coupled with active base line restorer (BLR)
BLR overshoot:	5–20%

Studies of the time-bin measurement width indicate that time bins about 3 ns (corresponding 3 bit subdivision of the 25 ns bunch crossing clock) offer an acceptable compromise between the measurement accuracy and data bandwidth requirements.

On the basis of the experience gained with the reference DC-coupled electronics these specifications for AC-coupled electronics were settled and a first 8-channel chip (ASDBLR) has been produced. This chip has been examined in laboratory and test-beam conditions and has shown very good operating properties:

- the measured analogue signal parameters are very close to the specified ones;
- the noise level is low enough to operate with the straw at the designed threshold of 200 eV and the nominal gas gain of (2.5×10^4);

- the chip is matched to the straw at minimum noise level due to dynamic input impedance implementation;
- the chip shows very good performance at high counting rate: drift-time measurement accuracy and efficiency at a threshold of 170 eV are degrade from 113 to 145 μm and from 89% to 62%, respectively, when the straw counting rate increases from 0 to 18.6 MHz.

Only minor improvements are needed to launch this chip into mass production.

Acknowledgements

We thank K. Bussmann and G. Di Tore for their valuable contributions to the preparation of mechanics and electronics for the tests. The research described in this publication was partly made possible owing to the following funding agencies: The European Union (DGXII), The International Science Foundation (grant NM5J000), The Swedish Natural Science Research Council, The Swedish Council for Planning and Coordination of Research.

References

[1] ATLAS inner detector technical design report, CERN/LHCC/97-17, ATLAS TDR 5, 30 April 1997.
[2] B. Dolgoshein et al., Nucl. Instr. and Meth. A 294 (1990) 473.
[3] V. Bondarenko et al., Nucl. Instr. and Meth. A 327 (1993) 386.
[4] T. Akesson et al., Nucl. Instr. and Meth. A 361 (1995) 440.
[5] T. Akesson et al., CERN-PPE/97-161, 11 November 1997.
[6] T. Akesson et al., Nucl. Instr. and Meth. A 367 (1995) 143.
[7] R.A. Boie, A.T. Hrisoho, P. Rehak, Nucl. Instr. and Meth. A 192 (1982) 365.
[8] B. Bevensee et al., IEEE Trans. Nucl. Sci. NS-43 (N3) (1996) 1725.
[9] M. Newcomer, A. Romaniouk, ATLAS Internal Note, INDET-NO-122, 1996.